Dimer reconstruction and electronic surface states on clean and hydrogenated diamond (100) surfaces

J. Furthmüller, J. Hafner, and G. Kresse
Institut für Theoretische Physik, Technische Universität Wien, Wiedner Hauptstrasse 8-10, A-1040 Wien, Austria
(Received 21 April 1995)

We present *ab initio* investigations of the structural and electronic properties of clean and hydrogen-covered diamond (100) surfaces within local-density-functional theory. Our calculations are based on a variational solution of the Kohn-Sham equations using a preconditioned conjugate-gradient approach and on the optimization of the atomic structure via a quasi-Newton quench based on the exact Hellmann-Feynman forces. The computations are performed in a plane-wave basis, the electron-ion interaction is described by optimized ultrasoft pseudopotentials. We find that the clean and the monolayer-covered surfaces reconstruct in a (2×1) cell via the formation of rows of symmetric π-bonded dimers. Further hydrogenation to a coverage of 1.5 ML stabilizes a surface with a (1×1) periodicity in the C layers, albeit with a low H-desorption energy for the formation of the reconstructed monohydride surface. The two-step desorption process is in good agreement with experimental observations. Electronic surface states within the bulk gap are predicted for the clean surface, but not for the monohydride case. The detailed analysis of the layer-resolved local densities of states and of the dispersion of the surface states demonstrates that the results are in good agreement with recent photoemission experiments. A negative electron affinity is predicted for the monohydride surface, but not for the clean surface.

I. INTRODUCTION

The structural and electronic properties of diamond surfaces have been the subject of an increasing number of experimental, theoretical, and computational studies. This interest is motivated by the evident importance of a precise knowledge of the properties of surfaces for further technological advances in the growth of nearly atomically smooth films via chemical vapor deposition (CVD) methods.[1–3] Among the three low-index surfaces of the tetrahedral semiconductors, the (100) orientation is of particular interest because atomically smooth surfaces have already been achieved by homoepitaxial CVD growth.[4] The (100) surface is also unique because each atom on the ideal surface has two dangling bonds while on the ideal (111) and (110) surfaces each atom has only one dangling bond. This leads to a very rich surface chemistry. A fully hydrogen-passivated (100)-(1×1) surface would contain two hydrogen atoms per carbon atom, but is supposed to be unstable due to the strong repulsion that exists between the hydrogen atoms. Loss of hydrogen leads to a reconstruction of the surface via the formation of C-C surface dimers. This reconstruction has also been observed experimentally.[5,6]

Theoretical studies of clean and hydrogenated diamond (100) surfaces have been performed using various empirical and semiempirical techniques.[7–15] The level of sophistication ranges from slab-MINDO (modified intermediate neglect of differential overlap)[9] and empirical tight-binding methods[7,13,15] to non-self-consistent local-density-functional (LDF) calculations.[12] These studies generally agree on the formation of dimers on the clean C(100)-(2×1) and monohydrogenated C(100)-(2×1):H surfaces, but there is considerable disagreement about the bond length of the dimer, whether the dimer is buckled or symmetric, and what is the hydrogen coverage for the fully passivated C(100)-(1×1):nH surface for which a (1×1) LEED (low-energy electron diffraction) pattern is observed.[6] The precise form of the dimer reconstruction of the diamond (100) surface is also of interest in relation to the reconstruction of the Si(100) and Ge(100) surfaces. For Si(100), conflicting evidence from theory and experiment indicates either symmetric or asymmetric dimers as the basic units of the room-temperature (2×1) and the low-temperature $c(4\times2)$ reconstructions.[16–23] The energy difference between the symmetric and asymmetric dimer reconstructions is predicted to be only 0.1 eV per dimer. Experimental evidence from scanning tunneling microscopy is possibly obscured by thermal flipping motions of the dimers between the right- and left-tilted positions.[20] For Ge(100), the asymmetric buckled dimers are energetically preferred.[24,25] Hence there seems to be a clear physical and chemical trend in the (100) surfaces of Ge, Si, and C: Ge(100) shows asymmetric dimers, Si(100) is a borderline case, and the C(100) surface probably shows symmetric dimers. Very recently, the physics of the dimer reconstruction of clean C(100) has been studied by *ab initio* LDF methods[26–28] and configuration-interaction Hartree-Fock (CI-HF) techniques.[29] The LDF calculations agree in predicting symmetric dimers with a very short bond length equal to the length of a double bond in a carbohydride molecule [d(C=C) = 1.37 Å], the absence of buckling is attributed to the large splitting between the bonding and antibonding surface states, which makes the Jahn-Teller-like symmetry breaking of the Si and Ge surfaces energetically unfavorable. The results of the HF calculations depend on the choice of the basis set and on the level of sophistication of the theory. At the level of single-determinant wave functions, symmetric dimers with a very large C-C bond length (d=1.68 Å) are predicted, CI calculations lead to symmetric dimers with a

still rather large bond length ($d = 1.52$ Å).[29]

The *ab initio* LDF predictions of strongly bonded symmetric dimers are in good agreement with the available experimental information on the clean C(100) surface. Lurie and Wilson[30] observed that the LEED pattern of C(100) surfaces changes from (1×1) to (2×1) after annealing at a high temperature of 1573 K. A similar conclusion was reached by Hamza, Kubiak, and Stulen[6] who emphasized that the reconstruction is not accompanied by a complete desorption of hydrogen, indicating a two-step reconstruction from a hydrogen-saturated unreconstructed C(100)-(1×1):nH surface (with an as yet undetermined coverage n) to a reconstructed C(100)-(2×1):H monohydride surface and further to an even more strongly reconstructed clean C(100)-(1×1) surface. However, quantitative information on the bond lengths in the reconstructed surfaces is not available. There have been several attempts to complement the incomplete structural information on the clean and hydrogenated diamond surfaces by investigations of their electronic properties.[6,31,32] For the C(111) surfaces the photoemission spectra indicate that besides the well-known surface configurations corresponding to the clean reconstructed surface and the monohydride-passivated surface, a third configuration is formed under extreme hydrogen exposure. This surface probably contains -CH_2 or -CH_3 groups at the surface.[31] The three configurations differ by the presence or absence of surface states in the vicinity of the Fermi level, as well as by differences in bulk states up to rather high binding energies. Similar changes have also been observed at the C(100) surfaces under repeated desorption and reloading with hydrogen.[6,31,32]

In this paper we present an investigation of the structural and electronic properties of clean and hydrogenated diamond (100) surfaces using *ab-initio* LDF techniques. Our approach is based on a variational solution of the Kohn-Sham equations of finite-temperature LDF theory in a plane-wave basis using preconditioned conjugate-gradient techniques and on the optimization of the atomic geometry using the exact Hellmann-Feynman forces.[33–35] The electron-ion interaction is described by optimized ultrasoft pseudopotentials[36,37] allowing for a low cutoff energy in the plane-wave expansion of the valence states. The use of the ultrasoft pseudopotentials solves the convergence problems[38] that plague many pseudopotential calculations for $2p$ elements such as C. The exact calculation of the Kohn-Sham ground state before each calculation of the Hellmann-Feynman forces eliminates the nonadiabaticity problems arising if the Fermi level falls into a partially occupied surface band. We have performed a full optimization of the clean and the monohydride surfaces and of a surface with 1.5 hydrogen atoms per C atom in the surface and we present a detailed analysis of the electronic structure of all three surfaces.

II. *AB INITIO* LDF METHOD

A. Variational solution of the Kohn-Sham equations and optimization of the atomic geometry

For our calculations we used the Vienna *ab initio* molecular-dynamics program (VAMP).[33–35] VAMP is based on the following principles:

(1) We use the finite-temperature version of LDF theory developed by Mermin,[39] with the exchange-correlation functional given by Ceperley and Alder as parametrized by Perdew and Zunger.[40] Finite-temperature LDF theory introduces fractional occupancies and a broadening of the one-electron energy levels (in the form of a Fermi-Dirac or a Gaussian broadening). This smearing helps to solve convergence problems arising from using a small set of $\vec{k}$ points for Brillouin-zone integrations, the use of fractional occupancies eliminates all instabilities that can arise from a crossing of levels in the vicinity of the Fermi energy. The variational quantity in finite-temperature LDF theory is the electronic free energy.

(2) The minimization of the free energy is performed using an efficient matrix-diagonalization routine based on a variant of the conjugate-gradient techniques developed by Payne and co-workers[41–44] and Bylander, Kleinman, and Lee.[45] The method is a doubly iterative one: in the inner loop the wave functions and eigenvalues at each $\vec{k}$ point in the Brillouin zone and for each band are improved at a fixed potential by a preconditioned conjugate-gradient (CG) method[45] until the change of the eigenvalue has dropped below a fixed threshold, i.e., the CG method is used as an instrument for the iterative calculation of the lowest eigenvalues ($\leqslant 10\%$ of all eigenvalues) of the large Hamiltonian matrix. After running over all bands (including some empty bands), a subspace diagonalization is performed, the Fermi energy and the new partial occupancies are recalculated, and the charge density and the potential are updated. For the large unit cells used in the slab calculations for the surfaces, it is essential to use an efficient mixing routine to avoid charge-sloshing problems. We use an improved Broyden mixing for calculating the new charge density and potential.[46–49]

(3) The optimization of the atomic geometry is performed via a conjugate-gradient minimization of the total energy with respect to the atomic coordinates. Alternatively, a full canonical molecular dynamics (MD) simulation may be performed using a Nosé thermostat for the ions.[34]

(4) After moving the atoms, the new charge densities are estimated by extrapolating the results of the last steps. A higher-order extrapolation requires a high accuracy in the calculation of the ground state.

(5) The calculation has been performed using a fully nonlocal optimized ultrasoft pseudopotential.[36,37] The nonlocal contributions are calculated in real space, using the optimized projectors introduced by King-Smith, Payne, and Lin.[42]

The program has been applied with good success to the crystalline, amorphous, and liquid phases of germanium,[34] to molten simple[35] and transition metals,[33] and to the investigation of the phase transitions between the layered, cubic, and high-pressure phases of carbon and boron nitride.[51] The most detailed description of the program is given in the paper by Kresse and Hafner.[34] A very important aspect of the application of the program to diamond is that it allows one to use ultrasoft pseudopotentials.

B. Ultrasoft pseudopotentials

Ultrasoft pseudopotentials have been introduced with the aim of reducing the number of plane waves necessary for a

well-converged expansion of the valence-electron states. Modern pseudopotentials are usually constructed from pseudo-wave-functions Φ_i (i is shorthand for all quantum numbers and for the energy of the reference state), fitted to the exact wave functions Ψ_i at a certain cutoff radius $R_{c,i}$ such that Φ_i is at least two times continuously differentiable at $R_{c,i}$ and that the norm of the wave function is conserved. The norm-conservation condition is thought to improve the transferability of the pseudopotential. Various attempts have been made to improve the accuracy and transferability of the potential and the convergence of the expansion of Φ_i in terms of plane waves by imposing further conditions on the pseudo wave functions.[52,53,55,54,36,37] Generally it turns out the pseudopotential can be softened by increasing the cutoff radius $R_{c,i}$, but the loss of accuracy and transferability puts an upper limit to $R_{c,i}$ and hence to a further reduction of the plane-wave basis set. It has been shown that in the case of diamond with accurate norm-conserving pseudopotentials a cutoff energy $E_{\rm cut}$ (corresponding to the highest kinetic energy of a plane wave in the basis) of 1000 eV is required to achieve full convergence.[51] Such a cutoff energy would require a number of plane waves per atom that is prohibitively large for simulations on large systems.

Vanderbilt[36] has pointed out that the main obstacle to a further increase of $R_{c,i}$ (and hence a reduction of $E_{\rm cut}$) is the requirement of norm conservation forcing the pseudo wave function to reproduce the sharp peak of the all-electron wave function (this concerns in particular the sharply peaked $2p$ wave functions of the first-row elements and the $3d$ wave functions of the transition metals). Dropping the norm-conservation constraint, however, makes the logarithmic derivative of the pseudo-wave-function deviate rather quickly from the all-electron value as the energy moves away from the reference value. Vanderbilt proposed improving the logarithmic derivative by fitting not just at one, but at least at two reference energies and to use a small set of localized ''augmentation functions'' to describe the charge-density deficit arising from the violation of the norm. It has been shown that with ultrasoft pseudopotentials for diamond, $E_{\rm cut}$ can be as low as 300 eV without any loss of accuracy.[37,51]

The new ''ultrasoft'' pseudo wave functions satisfy a generalized Kohn-Sham eigenvalue relation with an overlap operator given in terms of the augmentation functions. The existence of a nondiagonal overlap matrix must be considered in the calculation of the gradients of the wave functions. Due to the dependence of the overlap operator and of the augmentation functions on the positions of the ions, additional terms appear in the Hellmann-Feynman forces and in the stresses on the unit cell. The modifications of the *ab initio* MD routines introduced by the use of ultrasoft pseudopotentials are described in detail in Refs. 33, 37, 47, and 51.

For carbon, extensive tests of the optimal ultrasoft pseudopotential have been performed in Refs. 37 and 51. The optimal pseudopotential is specified by an atomic reference electron configuration $2s^2 2p^2$, cutoff radii $R_{c,s}=R_{c,p}=R_{c,d}=1.9$ a.u., and augmentation radii for the construction of the pseudized augmentation functions of $R_{{\rm aug},s}=1.3$ a.u., $R_{{\rm aug},p}=1.2$ a.u., and reference energies of $\epsilon_{s,1}=-13.84$ eV, $\epsilon_{s,2}=-9.52$ eV, $\epsilon_{p,1}=-9.52$ eV, $\epsilon_{p,2}=-5.31$ eV, and $\epsilon_d=-4.08$ eV (the d component of the pseudopotential is norm conserving). The d-electron pseudopotential was used as the local component. It is a characteristic feature of the ultrasoft pseudopotentials that large, even overlapping, cutoff radii can be used. Due to the description of the charge deficit in terms of the augmentation functions, the pseudo charge densities are still accurate. For a detailed study of the dependence on the cutoff radii, we refer to the earlier work on the phase stability of C.[51] We have shown[51] that calculations using this ultrasoft pseudopotential and a cutoff energy of $E_{\rm cut}=270$ eV lead to a maximal error of 0.003 eV/atom in the structural energy differences between the allotropic forms of carbon (diamond, graphite, bc8), compared to calculations with an optimized norm-conserving pseudopotential and a cutoff energy of $E_{\rm cut}=1100$ eV. For diamond, the calculated lattice constant and bulk modulus are 3.530 Å and 4.60 Mbar, to be compared with the experimental values of 3.567 Å and 4.43 Mbar, respectively. The remaining difference represents the characteristic LDF error. For consistency, the theoretical lattice constant has been used in the surface calculations.

For the hydrogen atom we have constructed an ultrasoft pseudopotential for the s component, while the p component was described by a norm-conserving potential. The cutoff radii are $R_{c,s}=R_{c,p}=1.25$ a.u. and the augmentation radius is $R_{{\rm aug},s}=0.8$ a.u. The reference electron configuration is $1s^1$ and the reference energies are $\epsilon_{s,1}=-6.36$ eV, $\epsilon_{s,2}=-9.52$ eV, and $\epsilon_p=-3.40$ eV. The pseudopotential was tested at the example of the H_2 dimer. The bond length, binding energy, and vibrational eigenfrequency of $d=0.765$ Å, $E_B=4.90$ eV, and $\omega=4210$ cm^{-1} are in good agreement with the experimental values of $d=0.74$ Å, $E_B=4.75$ eV, and $\omega=4395$ cm^{-1}.

III. COMPUTATIONAL ASPECTS OF THE MODELING OF THE DIAMOND (100) SURFACE

We have modeled the diamond surfaces by a finite slab consisting of eight layers of eight C atoms each [corresponding to a (4×2) surface cell], separated by eight layers of vacuum. A (4×2) cell is necessary to investigate the possibility of a higher-order reconstruction than (2×1) such as that found in the low-temperature phases of Si(100).[19] A supercell containing 64 atoms corresponds well to the state-of-the-art of *ab initio* LDF calculations for both silicon[17,20,23] and diamond.[28] For some tests, the calculations have been extended to 16-layer slabs and a wider vacuum layer. These tests show clearly that the surface geometries obtained with the eight-layer slabs are unchanged if the thickness of the layer is doubled. For most calculations, the coordinates of the lowest double layer were fixed in the ideal bulk-terminated geometry to simulate the bulk material. Test calculations have also been performed with symmetric layers. Even for the eight-layer slab we found that the interaction of the surface states across the layer caused a maximum splitting of the symmetry-degenerate surface states on both sides of the slab of a few meV. We also verified that increasing the thickness of the slab to 16 layers did not change the energies of the surface states by more than a few meV.

For the hydrogenated surfaces, a layer with eight or twelve H atoms was added to the topmost C layer. The positions of the atoms in the lowest C layer are kept fixed to simulate the bulk material. The pseudo-wave-functions and

the smooth part of the charge density and potential are calculated on a $32\times32\times64$ fast-Fourier-transform grid, a finer $48\times48\times96$ grid was used for the augmentation functions and charges in the ultrasoft pseudopotential scheme (the finer grid in $\vec{r}$ space is used for calculating the Hartree and exchange-correlation potentials only). These grids correspond to cutoff wave vectors of $G_{\rm cut} = 7.53$ and 11.30 a.u., respectively. For the Brillouin-zone integrations we used a $2\times2\times1$ grid of Monkhorst-Pack special points,[56] together with a Gaussian broadening of $\sigma = 0.1$ eV in the finite-temperature LDF scheme[34,57,58] during the atomic relaxation calculations. For the calculation of total energies, an extrapolation to $\sigma\rightarrow 0$ has been performed.[57] For the determination of the reconstructed geometry, the atomic coordinates were relaxed via a quasi-Newton-quench.[48] For the calculation of the electronic density of states and of the electronic eigenstates and charge densities of the equilibrium atomic configurations, a minimal (2×1) cell with 16 C atoms (eight layers with two C each), plus 0, 2, and 3 H atoms and a finer $8\times16\times3$ Monkhorst-Pack grid was used. The iterative calculation of the Kohn-Sham eigenstates is stopped when the eigenvalues are converged to within 0.1 meV. The optimization of the atomic coordinates was continued until the total energy was converged to within 1 meV/atom. Layer-resolved local densities of states have been calculated on the basis of a projection of the plane-wave components of the eigenstates onto spherical waves within the individual atomic spheres,[59] this projection technique has also been used for the analysis of electronic surface states.

IV. OPTIMIZATION OF THE SURFACE GEOMETRY

In our study we investigated five different surfaces: (a) the clean C(100)(1×1) surface (only vertical relaxation of rigid layers allowed), (b) the clean reconstructed C(100)(2×1) surface, (c) the monohydrogenated unreconstructed, but relaxed C(100)(1×1):H surface, (d) the reconstructed monohydride surface C(100)(2×1):H, and (e) a surface covered with 1.5 monolayers of hydrogen with the hydrogen atoms arranged in alternant rows of monohydride and dihydride units, C(100)(1×1):1.5H [note that the (1×1) periodicity refers to the C layers only].

A. Clean C(100)(1×1)

For the clean surface with the ideal geometry of the bulk lattice we calculate a surface energy (cleavage energy) of 3.89 eV/surface site. The relaxation of the surface layers within a restricted (1×1) geometry leads to a modest energy gain of $\Delta E = 0.26$ eV/surface atom, the distance between the C atoms in the surface layer (S) and the first subsurface layer ($S1$) is reduced from $d_{12}(C-C) = 1.53$ Å in the ideal bulklike geometry to $d_{12}(C-C) = 1.47$ Å.

B. Clean C(100)(2×1)

The reconstruction of the clean C(100) surface leads to the formation of rows of symmetric dimers with a bond length of $d_{11}(C-C) = 1.37$ Å, i.e., almost equal to the length of the C=C double bond in the C_2H_4 molecule ($d=1.38$ Å). Details of the reconstructed geometry are given in Fig. 1. The distance between the S and ($S1$) atoms

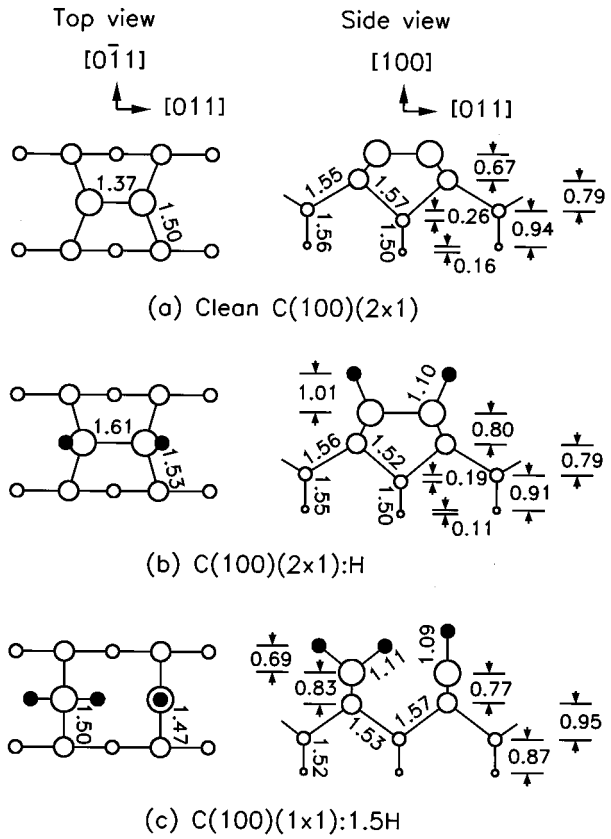

FIG. 1. Top views and side views of the reconstructed C(100)(2×1) (a), the reconstructed hydrogenated C(100)(2×1):h (b), and of the higher H-loaded C(100)(1×1):1.5H (c) surfaces [note that for the last surface the periodicity (1×1) refers only to the carbon layers and not to the hydrogen adlayer]. The numbers along the connecting lines marking the nearest-neighbor bonds represent the bond lengths (in Å). The other distances (marked by the lines enclosed between arrows) are the vertical distances between the C atoms in adjacent layers or within a buckled layer (again given in Å); cf. text.

[$d_{12}(C-C) = 1.50$ Å] is slightly increased relative to the (1×1) surface, but still smaller than in the bulk. Together with the short surface dimers, this leads to an appreciable inwards relaxation of the surface layer. The reconstruction also induces a considerable buckling of the ($S2$) and ($S3$) layers (by 0.26 and 0.16 Å , respectively) because there are now two inequivalent C sites in each layer (one just below the surface dimers and one below the intervals between the dimers). The two ($S2$) to ($S3$) bond lengths are 0.03 Å larger (smaller) than the bond length in the bulk. Our calculations have been performed with a (4×2) surface cell, but the forces acting on the atoms give no indication for a higher-order reconstruction than (2×1).

Our calculated surface geometry is in excellent agreement with two other recent *ab initio* LDF calculations;[27,28] see the compilation in Table I. The non-self-consistent tight-binding (TB) calculations[12,13,15] predict a 0.03–0.04 Å larger bond length in the dimer, and eventually a slight buckling of the dimers.[12] Buckling was also predicted by the earlier TB calculations of Reichardt and Bechstedt.[7] These discrepancies indicate the uncertainty arising from the construction of the TB Hamiltonian. The important point is that all *ab initio*

TABLE I. Bond lengths (in Å) in reconstructed (relaxed) C(100) surfaces.

	Present work	Ref. 27 [a]	Ref. 28 [b]	Ref. 12 [c]	Ref. 15 [d]	Ref. 15 [d]	Ref. 13 [e]	Ref. 10 [f]	Ref. 9 [g]
(2×1)									
C=C dimer	Symmetric	Symmetric	Symmetric	Buckled	Symmetric		Symmetric	Symmetric	Symmetric
d_{11}(C-C)	1.37	1.37	1.37	1.40	1.40		1.41	1.58	1.38
d_{12}(C-C)	1.50	1.50		1.52			1.50		1.48
				1.55					
(2×1):H									
d (C-H)	1.10			1.17	1.12		1.07	1.08	1.13
C=C dimer	Symmetric			Symmetric	Symmetric		Symmetric	Symmetric	Symmetric
d_{11}(C-C)	1.61			1.67	1.62		1.58	1.73	1.56
d_{12}(C-C)	1.53			1.59			1.54		
(m×1):nH									
n,m	1.5,1			1.33,3	1.5,2	2,1	1.5,1	2,1	
d(C-H), monohydride	1.09			1.18	1.12		1.07		
d(C-H), dihydride	1.11			1.17	1.27 [h]	1.07	1.07	1.08	
d_{11}(C-C), dimer	2.50			1.62	2.36	2.51			
d_{12}(C-C), monohydride	1.47			1.58			1.48		
d_{12}(C-C), dihydride	1.50			1.60			1.52		

[a]Kress *et al.*, *ab initio* LDF.
[b]Krüger and Pollmann, *ab initio* LDF.
[c]Yang *et al.*, non-self-consistent DFT-TB.
[d]Davidson and Pickett, TB molecular dynamics.
[e]Frauenheim *et al.*, TB molecular dynamics.
[f]Mehandru and Anderson, molecular orbital.
[g]Zheng and Smith, MINDO.
[h]The 1.5-fold hydrogenated surface of Ref. 15 corresponds to single H atoms bonded to the C atoms, with pairs of C atoms sharing a common H atom in a symmetric position.

calculations predict that there is no buckling of the surface dimers, in contrast to the Si(100) (Ref. 20,22, and 23) and Ge(100) surfaces.

The calculated reconstruction energy is $\Delta E = -1.51$ eV/site relative to the relaxed (1×1) surface, reducing the surface energy to 2.12 eV/site. Again we find good agreement with *ab initio* LDF and semiempirical TB calculations (cf. Table II). It is remarkable that for the clean surface, the reconstruction energy per dimer is larger than the cohesive energy per bulk bond ($\Delta E = 3.02$ eV/dimer, $E_{\rm coh} = 2.25$ eV/bond). This reflects the strength of the double bond in the dimer. The reconstruction energy calculated for C(100) is considerably larger than that obtained for the Si(100) surface where Vittadini *et al.*[22,60] find the buckled dimer configuration to be ~ 0.80 eV/site lower in energy than the (1×1) bulk-terminated surface and ~ 0.15 eV/site lower than the (2×1) symmetric-dimer structure. The much higher reconstruction energy reflects the strength of the C=C double bond.

C. Monohydride C(100)(2×1):H surface

If the surface is covered with a monolayer of hydrogen (one hydrogen atom per carbon atom in the surface), the reconstruction pattern changes only quantitatively: the length of the surface dimers is now $d_{11}(C-C) = 1.61$ Å, i.e., slightly larger than a single C-C bond in a hydrocarbon molecule [$d(C-C) = 1.55$ Å in C_2H_6], the S-($S1$) bond length is close to the bulk value so that the inwards relaxation of the

TABLE II. Reconstruction energy ΔE (in eV per surface site) and hydrogen-adsorption energy $\Delta E_{\rm H}$ (in eV per H atom, see also text) for C(100) surfaces.

		Present work	Ref. 23	Ref. 24	Ref. 10	Ref. 11	Ref. 8	Ref. 7
ΔE	C(100)(2×1)	-1.51	-1.76	-1.68	-1.82	-1.50	-1.84	-3.93
	C(100)(2×1):H	-0.91						
$\Delta E_{\rm H}$	C(100)(1×1):H	-5.14						
	C(100)(2×1):H	-4.54			-6.20		-6.63	-6.32
	C(100)(m×1):nH	-1.02			-3.90		-2.44	-4.11
		$n=1.5$			$n=1.33$		$n=2$	$n=2$
		$m=1$			$m=3$		$m=1$	$m=1$

top layer is now very small. The buckling of the deeper subsurface layers is reduced (see Fig. 1 and Table I for details). The C-H bond length $d(C-H) = 1.10$ Å.

There are no other *ab initio* calculations of the hydrogenated surface. The TB-based calculations[12,13,15] predict C-H bond lengths varying between $d(C-H) = 1.07$ Å and $d(C-H) = 1.17$ Å, and dimer bond lengths varying between $d_{11}(C-C) = 1.58$ Å and $d_{11}(C-C) = 1.67$ Å, i.e., they agree with the *ab initio* results within the limited accuracy of the TB theory.

The reconstruction energy per dimer is now $\Delta E = -1.81$ eV/dimer, i.e., smaller than the cohesive energy per bond. The H adsorption energy ΔE_{H} per H atom is defined as the energy difference between the hydrogenated, reconstructed surface and the clean, reconstructed surface plus a free H atom per surface site. Our value of $\Delta E_{\mathrm{H}} = -4.54$ eV/surface site (including the effect of the spin polarization of the free atom) is nearly 2 eV smaller than earlier TB predictions. The ΔE_{H} defined in this way measures the activation energy necessary to break the C-H bond. As the desorbed H atoms immediately recombine to form H_2 molecules, the total energetic cost of the desorption reaction is $\overline{\Delta E_{\mathrm{H}}} = 2.05$ eV/surface site, defined as the energy difference between the hydrogenated diamond surface and the clean surface plus molecular hydrogen.

Again it is instructive to compare the hydrogen-induced changes in the surface structure with the results obtained for the silicon surfaces. For Si(100)(2×1):H, Northrup[17] and Vittadini *et al.*[22,23] predict from *ab initio* LDF calculations the disappearance of buckling upon hydrogenation. However, the increase of the dimer bond length is only 0.16 Å on Si(2×1) compared to 0.24 Å on C(2×1). Also, the length of the Si-H bond of 1.55 Å is much greater than that of the C-H bond. Both effects point to a very strong C-H interaction.

D. Higher hydrogen coverage

There is now a general agreement that the C(100) surfaces showing a (1×1) LEED pattern are passivated by more than one monolayer of hydrogen, but there is disagreement as to the exact amount of hydrogen necessary to induce a complete dereconstruction. A saturation of all dangling bonds would require a coverage of two hydrogen atoms per surface sites. Such a high coverage was considered in the molecular orbital studies of Mehandru and Anderson[10] and in the recent TB calculations of Davidson and Pickett[15] (see Table I), but other calculations (e.g., Frauenheim *et al.*[13]) lead to the result that such a high coverage is unstable because of the strong repulsion between the H atoms placed at such short distances.

In our calculations we have studied in detail a surface covered by 1.5 monolayers (ML) of hydrogen, with alternant rows of C atoms bonding one and two H atoms, respectively. The relaxed geometry of this surface is very close to, but not exactly equal to (1×1): the S and ($S1$) layers are slightly buckled, but the lateral distances are exactly equal to the bulk values (see Fig. 1 and Table I). The relaxation of the slab was started from different configurations [including the ideal (1×1) geometry and several configuration with a broken surface symmetry], but the final result was always the "pseudo"-(1×1) surface. The predicted geometry is in good agreement with the results of Frauenheim *et al.*[13] The main difference is that we find slight differences in the lengths of the monohydride and dihydride bonds (which is reasonable), whereas the bond lengths are equal in the TB calculation. Davidson and Pickett considered a different geometry for the 1.5-layer coverage: monohydride bonds at all C surface sites, with the extra H atoms in symmetric interstitial surface sites. As the distance between the C atoms and the extra H atoms is rather large [$d(C-H) = 1.27$ Å], the bonding must be rather weak. Yang, Drabold, and Adams[12] considered a C(100)(3× 1):1.33H surface consisting of alternating C-C dimers (with one H atom per C atom in the dimer) and dihydride units leading to a (3× 1) surface periodicity. Evidently, a higher than monolayer coverage allows for a very large number of different surface structures.

Unfortunately, the energetics of H adsorption has hardly been explored in previous calculations. We find that an increase of the H coverage from 1 to 1.5 ML proceeds at an adsorption energy of $\Delta E_{\mathrm{H}} = -1.02$ eV per H atom. This is very small compared to the adsorption energy of $\Delta E_{\mathrm{H}} = -4.54$ eV per H atom for the formation of the first monolayer. Our result is in good agreement with the temperature-programmed desorption experiments of Hamza, Kubiak, and Stulen.[6] They found that H desorption from a strongly H loaded C(100) surface occurs in a two-step process. The first desorption step has an activation energy of 1.61 eV per H atom and leads to a still H-covered surface with (2×1) symmetry. Further H desorption requires much higher activation energies. Previous semiempirical calculations have predicted much higher desorption energies for the first step (see Table I).

Again it is instructive to draw a comparison with the strongly hydrogenated silicon surfaces. Based on scanning-tunneling microscopy, Boland[61] suggested for Si(100) the existence of an ordered (3×1) phase with a coverage of 1.5 monolayers (arranged in the form of alternating monohydride and dihydride units), and of a possibly disordered (1×1) phase with a coverage of 2 ML hydrogen. *Ab initio* calculations by Northrup[17] and Vittadini *et al.*[22] indicate that the Si(3×1):1.33H phase is stable over a certain limited range of the hydrogen chemical potential. For dihydride coverage, a structure with canted dihydride units is found to be more stable than the symmetric bulklike configuration. The structure proposed for the (3×1) phase is that investigated by Yang *et al.* for C(100)(3×1):1.33H. However, it is improbable that the "canted row" structure found for Si (1×1):2H is stable for the dihydrogenated C(100) surface. In the case of Si(100), the canting allows one to increase the shortest H-H distances from 1.51 to 2.21 Å, and this appears to be sufficient to reduce the Coulomb repulsions. With the much smaller interatomic distances on the diamond surfaces, the Coulomb repulsion is still to a high even after canting. Preliminary results from simpler tight-binding molecular-dynamics calculations on much larger C(100) surface cells suggest the existence of complex higher-order reconstructions.[62] However, in view of our remarks on the limited accuracy of tight-binding calculations, an at least punctual verification of these predictions by *ab initio* calculations appears to be necessary.

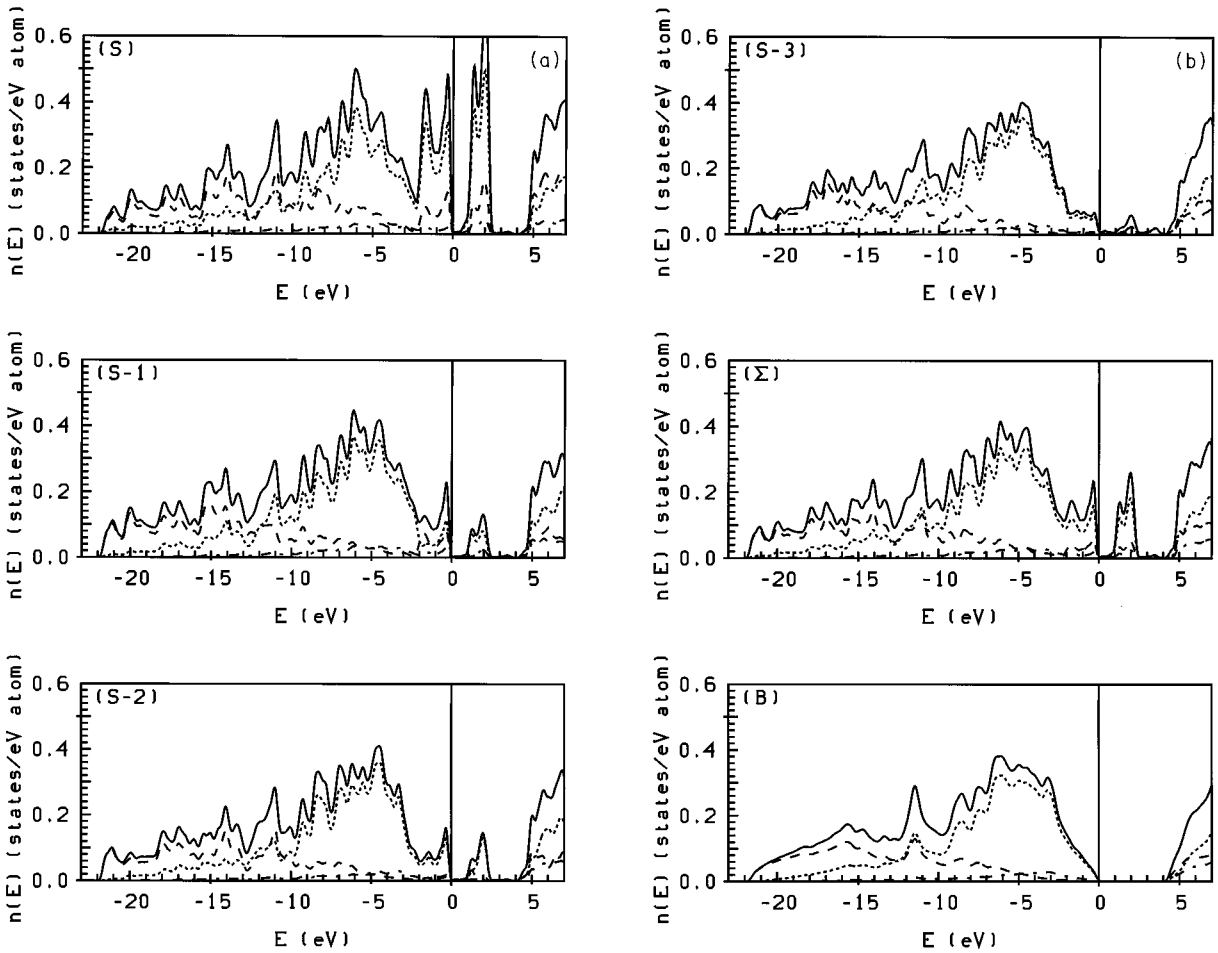

FIG. 2. Layer-resolved density of states (DOS) in the surface (S) and the first three subsurface ($S1$, $S2$, $S3$) layers, together with the bulk density of states (B) and the DOS integrated over the first four layers [Σ(1-4)] for the clean C(100)(2×1) surface. The full lines represent the total DOS, the dashed and dotted lines the s- and p-electron partial DOS's.

V. ELECTRONIC PROPERTIES

Whereas the electronic properties of the (111) surfaces of natural as well as CVD grown diamond have been investigated intensively using both experimental and theoretical techniques, less attention has been devoted to electronic states on the C(100) surfaces. For the clean C(111)(2×1) surface of natural diamond, photoemission spectroscopy (PES) and angular-resolved photoemission[63] have demonstrated the existence of electronic surface states covering an energy range of 2 eV and exhibit a maximum emission intensity at 1 eV below the valence-band maximum in normal emission (i.e., at the center of the surface Brillouin zone). In off-normal emission an upwards dispersion of about 1 eV has been found. The extra emission intensity associated with the surface states disappears after hydrogen loading and the transformation to a (1×1) symmetry. Similar reversible changes on H desorption and reloading have also been found on CVD-grown diamond films.[31] Electronic surface states on C(111) have also been studied by *ab initio* techniques.[64,65] Theoretical as well as experimental studies point to a pronounced similarity of the electronic surface states on C(111) with those on the corresponding Si surface. For Si, *ab initio* studies have been performed for the clean and hydrogenated (111) (Refs. 66 and 67) and (100) (Refs. 20, 22, and 23) surfaces. The common feature is that the passivation of the dangling bonds at the surface moves the surface states in the gap into the valence and the conduction band, respectively.

For the clean C(100)(2×1) surface preliminary photoemission experiments by Hamza, Kubiak, and Stulen[6] have demonstrated the existence of occupied electronic surface states within an interval of 2 eV from the valence-band maximum. The existence of surface states close to the upper edge of the valence band has been confirmed by recent photoemission studies by Oelhafen and Francz[32] who showed that the surface-related features appear only after annealing at 1250 K and vanish again after reloading with hydrogen. However, there are appreciable discrepancies as to the precise position of the surface states. Preliminary information is also available on the dispersion of the electronic surface states.[32,68] If the sample is tilted away from normal incidence, the surface-related peak becomes weaker and splits into two features showing strong and weak dispersion. Some information on electronic surface states is also available from recent *ab initio* calculations,[26–28] the TB calculations of Yang, Drabold, and Adams[12] and Davidson and Pickett[15] and our own preliminary *ab initio* studies[26] have extended the investigations to the hydrogenated surfaces. There is general agreement that surface states in the bulk gap exist for the clean, reconstructed surface, but not after monolayer passivation. These results are in qualitative agreement with the PES studies.

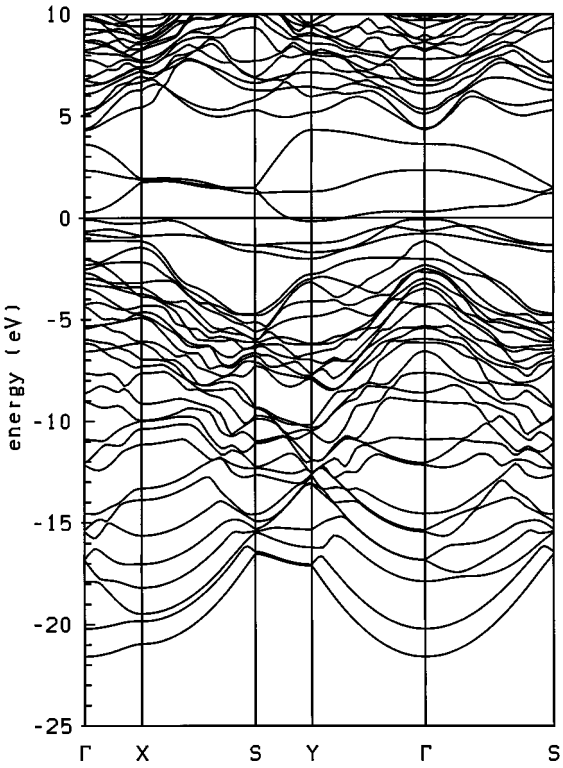

FIG. 3. Dispersion relations of the electronic eigenstates of an eight-layer C(100) slab with the lower surface fixed in the ideal bulk geometry and a clean, reconstructed upper surface. See text.

Little is known about the electronic properties of the heavily hydrogenated samples.

It has also been suggested that negative-electron-affinity (NEA) effects can be observed at the C(100) surface.[69] NEA surfaces are semiconductor surfaces that have a work function such that the vacuum level lies below the conduction-band edge. A NEA has been found on C(111) surfaces[70,71] and has been associated with the presence of hydrogen bonded to the surface. The recent PES work of van der Weide *et al.*[69] indicates that a NEA occurs also for a hydrogen-terminated C(100) surface with a (2×1) LEED pattern.

A. Clean C(100)(2×1)

1. Total and layer-resolved densities of states

We begin by analyzing the total and layer-resolved densities of states (DOS). The following figures display the local DOS (total and decomposed in to the *s* and *p* contributions) in the top four *C* layers (plus eventually the *H* layer) and the sum of the local DOS for these layers. For comparison the bulk DOS is also shown. The DOS' have been calculated using the small (2×1) cell with a fine $8\times16\times3$ grid and the tetrahedron method. The local projector technique described above has been used for the layer-resolved DOS's. The DOS of the clean C(100)(2×1) surface is shown in Fig. 2. The DOS of the surface layer shows the presence of both occupied and empty surface states in the bulk gap. The occupied surface states extend over an energy range of about 2 eV below the valence-band maximum, with two peaks at 0.5 and

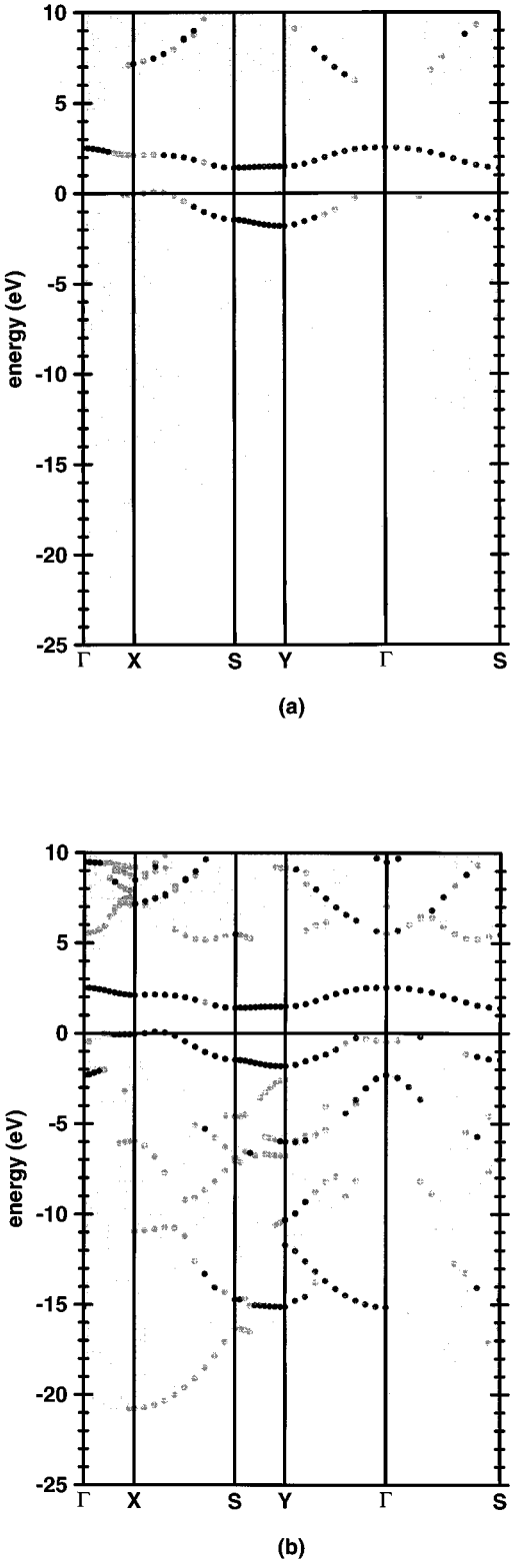

FIG. 4. Dispersion relations of electronic surface states on clean, reconstructed C(100)(2×1). The shaded areas represent the projected band structure of bulk diamond. The full circles represent surface states, the degree of shading corresponds to the degree of localization in the surface. In part (a) states with more than 45% (60%, 75%, 90%) of the total intensity in the surface (S) layer are considered as surface states. In part (b), the same criterion has been applied to the sum of the intensities in the S and ($S1$) layers. See text.

1.7 eV below the valence-band maximum. In the bulk gap, a band of empty surfaces states is situated between 1.5 and 2.5 eV above the valence-band maximum. The DOS related to the surface states is predominantly of p character. The surface-related features in the DOS extend, albeit with strongly reduced intensity, to the first and second subsurface layers, the DOS of the ($S3$) layer is already close to the bulk DOS.

2. Surface states

Figure 3 shows the complete set of bands calculated for an eight-layer slab with clean surfaces. The upper surface has been reconstructed, while the lower surface is fixed in the ideal bulk geometry. The calculation has been perfomed for a (2×1) unit cell on the surface; the bands are drawn along a path of symmetry lines in the tetragonal (2×1) surface Brillouin zone. The picture is confusing because it contains two different types of surface states: those of the clean, unreconstructed lower surface and those of the strongly reconstructed upper (2×1) surface. The analysis of surface states requires their precise definition according to an appropriate criterion. Figures 4(a) and 4(b) show the projected band structure of the bulk (the shaded areas) and the dispersion relations of the surface states. In part (a) a state has been considered as a surface state if more than 45% of its intensity is concentrated in the surface layer. It is represented by a filled circle whose shading indicates the degree of localization (more than 45%, 60%, 75%, and 90%, respectively). We shall refer to this mode of defining surface states as criterion 1. Part (b) represents the surface states obtained if the same criterion is applied to the S and ($S1$) layers (criterion 2). We find that only the two surface bands within the bulk gap are genuine surface states that are strictly localized in the first layer. The maximum of the occupied surface band is situated close to the X point; the band shows almost no dispersion along $\overline{\Gamma X}$, but strong dispersion along the $\overline{\Gamma S}$ and $\overline{\Gamma Y}$ directions. The surface band gap is about 1.2 eV between the maximum of the occupied band along $\overline{XS}$ and the minimum of the empty band along $\overline{SY}$. A number of surface resonances and surfaces states split from the bulk bands are identified using criterion (2).

The two surface bands within the bulk gap are mainly related to dangling bonds parallel to the surface, as demonstrated by the charge-density analysis in Fig. 5. The occupied (unoccupied) surface bands in the bulk gap are formed by bonding π (antibonding $\pi^\star$) linear combinations of dangling p orbitals centered at the C atoms forming the surface dimers, modified by rehybridization with the p orbitals parallel to the surface [see Figs. 5(a) and 5(b) representing the charge densities of the occupied and empty surface states at the S point]. Upon formation of the dimer bond, the splitting of the σ and $\sigma^\star$ states is much larger than the π-$\pi^\star$ splitting so that electrons are transferred from the $\sigma^\star$ to the π and $\pi^\star$ orbitals, resulting in the formation of bonding and antibonding states that are asymmetric with respect to the axis of the dimer. A similar hybridization mechanism for the surfaces states has already been discussed by Mehandru and Anderson.[10]

Surface states at higher binding energy (within the range of the bulk bands) correspond to σ bonds between the S and ($S1$) C atoms [see Figs. 5(c) and 5(d)] and to σ bonds in the dimer.

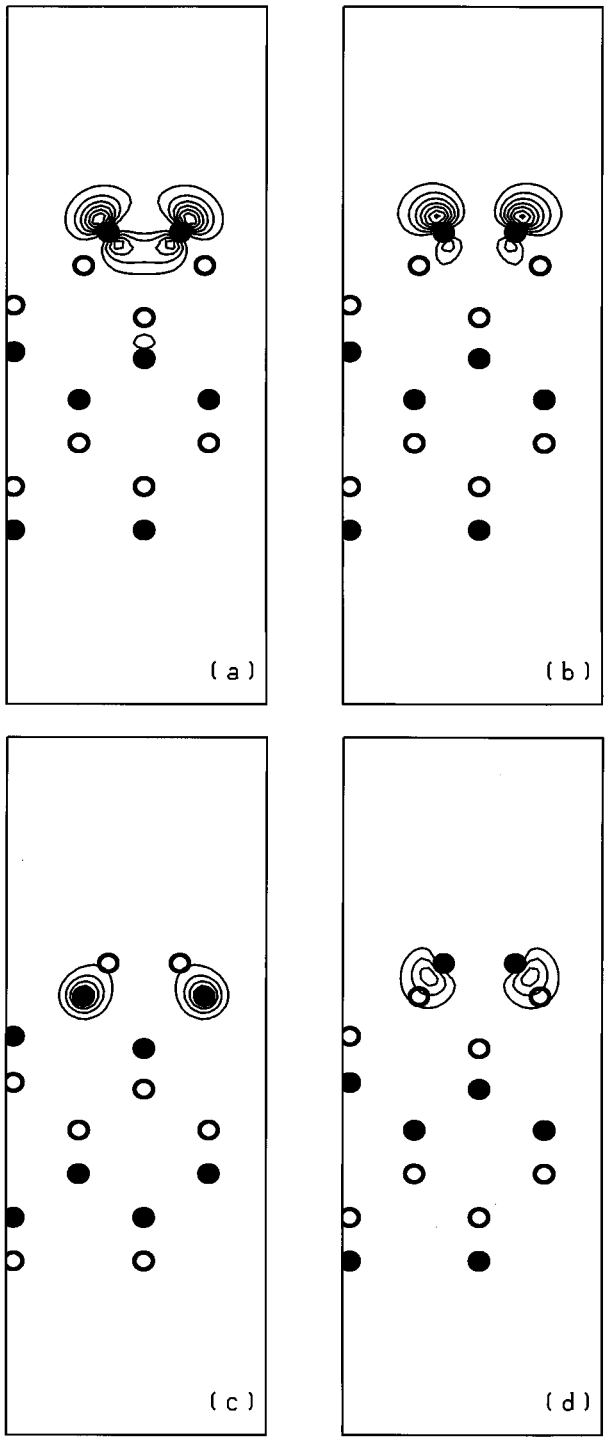

FIG. 5. Charge-density distributions for surface states on C(100)(2×1). (a) Occupied bonding π state at the S point and $E=-1.5$ eV; (b) unoccupied antibonding $\pi^\star$ state at the S point and $E=1.5$ eV; (c),(d) most localized surface states within the bulk bands, at the Γ point and $E=-2.2$ eV binding energy (c) and at the Y point at $E=-10.4$ eV binding energy (d). Cf. Fig. 4 and text. Contour lines are drawn at intervals of 0.1 electrons $\times$ Å^{-3}. Filled and empty circles represent C atoms in and below and above the drawing plane, respectively.

The C(100)(2×1) surface band structure is only qualitatively similar to that calculated for the Si(100)(2×1)

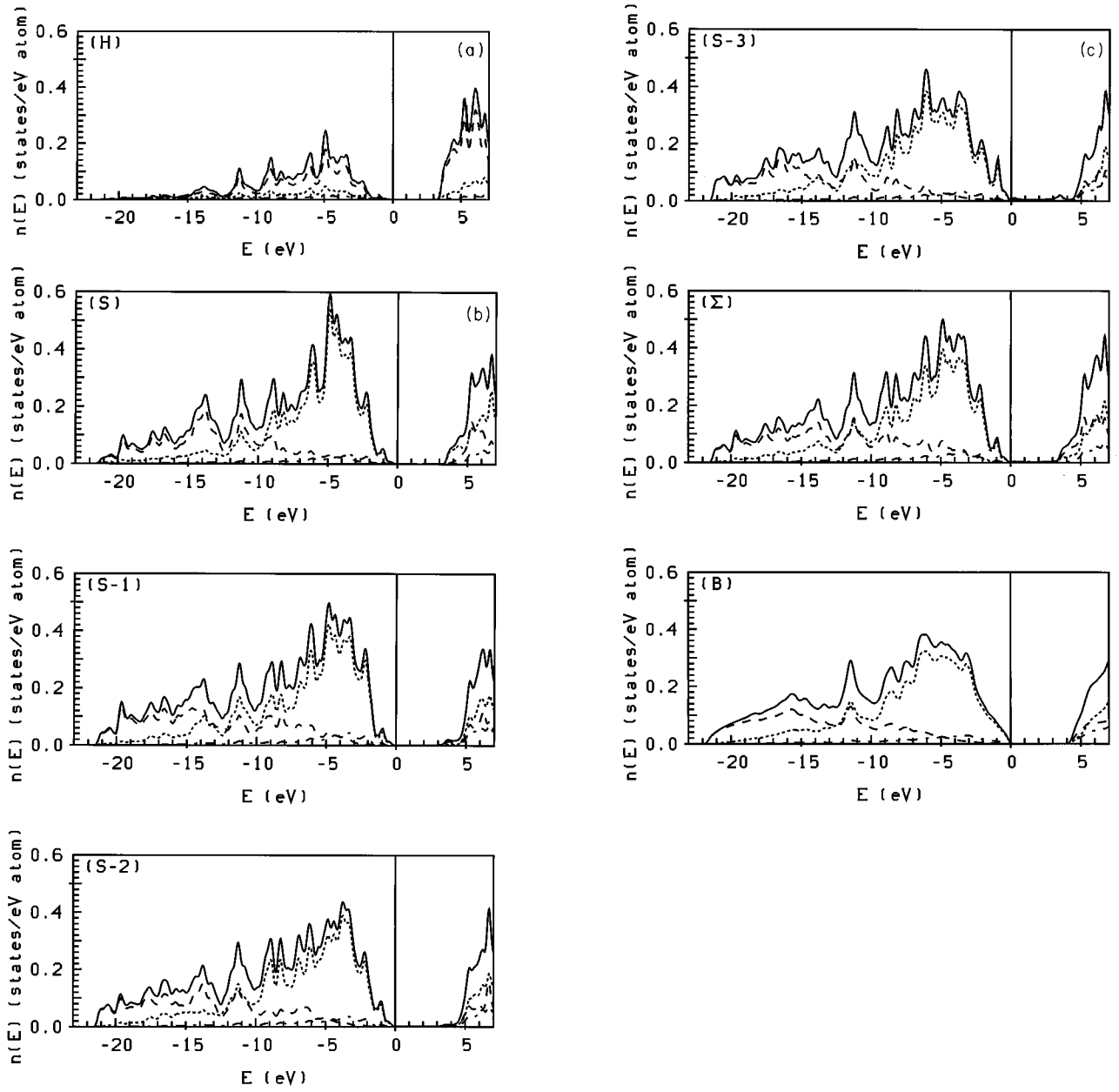

FIG. 6. Layer-resolved total and partial densities of states for the C(100)(2×1):H surface. We show the DOS's in the H layer (H), the top four C layers [S, ($S1$), ($S2$), ($S4$)], their sum (Σ), and for comparison the bulk DOS (B). Full line: total DOS; dashed line: *s*; dotted line: *p* partial DOS.

surface.[20,73] In the case of diamond, there is an indirect gap of about 1.2 eV between the filled π band and the empty $\pi^\star$ band. The π band shows a dispersion of about 2 eV across the surface Brillouin zone, the $\pi^\star$ has a weaker dispersion of about 1.2 eV. For the Si and Ge (100) surfaces with a symmetric dimer reconstruction, the π and $\pi^\star$ bands overlap. This would mean that the surfaces are metallic, in marked contrast to experiment. For the Si and Ge surfaces, a Jahn-Teller-like distortion of the surface structure leads to asymmetric dimers, the asymmetry leads to a splitting of the surface bands and the formation of a semiconducting surface, as discussed by Krüger and Pollmann.[28] For C(100) the gap between the occupied and empty surface states exists already for the symmetric dimers, the bonding or antibonding interaction is too weak to lead to a buckling of the surface dimers.

Our results are in very good agreement with the *ab initio* calculations of Krüger and Pollmann[28] and Kress *et al.*[27] and are consistent with the TB-LDF calculations of Yang, Drabold, and Adams,[12] but differ appreciably from the semiempirical TB calculations of Davidson and Pickett,[15] Frauenheim *et al.*[13] and Gavrilenko.[74] Gavrilenko's results show only a single occupied surface level in the gap. Davidson and Pickett find two surface states in the gap, but the minimum of their π state lies more than 1 eV above the valence-band maximum, whereas the *ab initio* calculations (Refs. 27,28, and present work) agree in predicting a π band whose maximum agrees with the top of the valence band. Also the splitting of the π and $\pi^\star$ states is 2.7 eV, i.e., more than twice as large as the *ab initio* LDF prediction. Here we have to re

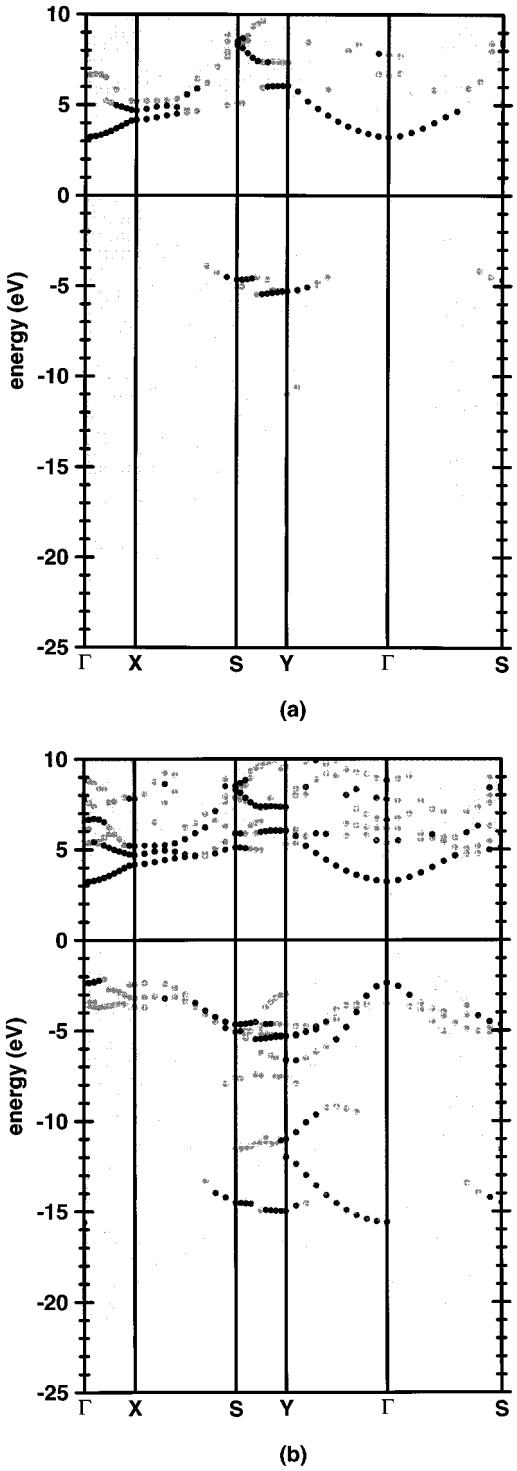

FIG. 7. Dispersion relations for electronic surface states on a reconstructed C(100)(2×1):H monohydride surface, defined according to criteria (1) [part (a)] and (2) [part(b)]. For the explanation of symbols, see Fig. 4 and text.

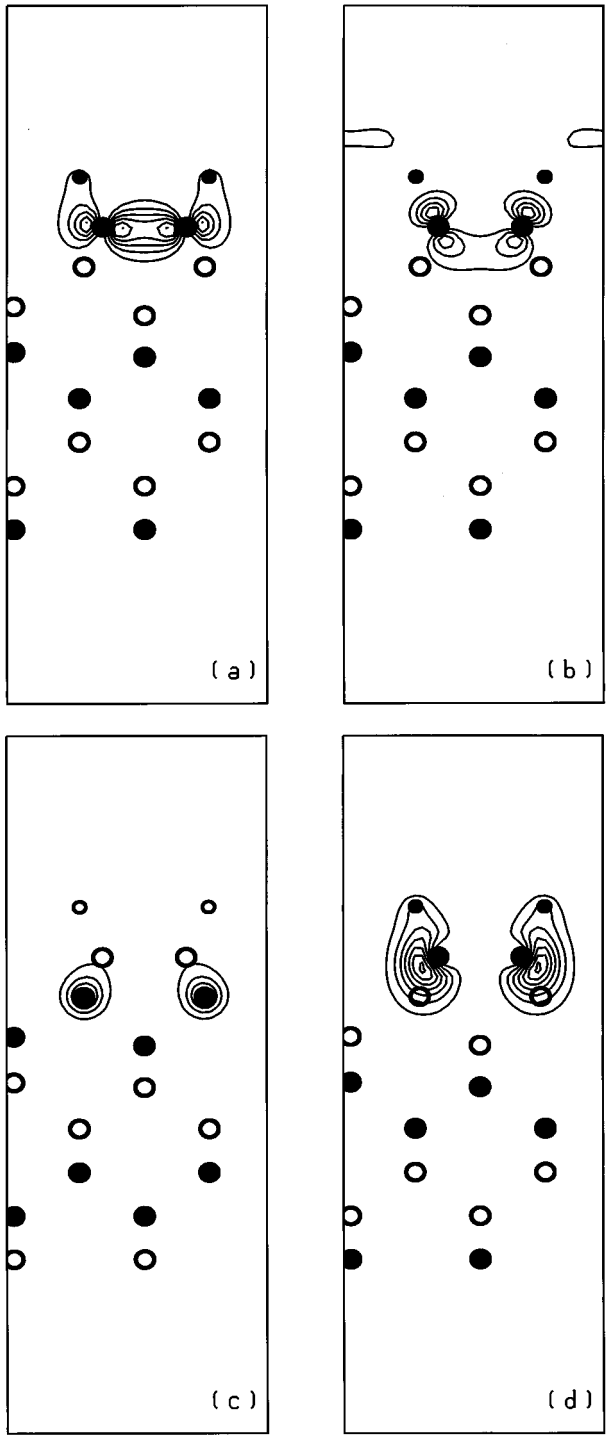

FIG. 8. Charge-density distributions for surface states on C(100)(2×1):H. (a) Occupied σ surface state at the S point and $E=-4.7$ eV binding energy, (b) lowest empty surface state at the Γ point and $E=3.2$ eV; (c),(d) occupied surface states at the Γ point and $E=-2.2$ eV and at the Y point and $E=-11$ eV (cf. also Fig. 5). Contour lines are drawn at intervals of 0.1 electrons/Å^3 in parts (a) and (c), and 0.04e/Å^3 for (b) and (d). Large circles represent C atoms and smaller circles represent the absorbed H atoms.

member that the LDF eigenvalues have a restricted meaning, especially as far as the prediction of electronic excitation energies is concerned. Characteristically, the LDF prediction of the gap width is below the experimental value: for bulk diamond we have $E_g = 4.25$ eV (LDF, from Γ to $\sim 0.8X$),[26] and $E_g = 5.47$ eV (experiment[75]). Kress *et al.*[27] have performed quasiparticle calculations of the electronic excitation energies on the reconstructed C(100) surface in Hedin's *GW* approximation.[76,77] They find that the quasiparticle corrections increase the bulkgap by 1.65 eV; the surface gap is increased to 2.14 eV by moving the π^* band to higher energies, but without affecting their dispersion in a signifi-

cant way. However, the unoccupied surface band remains within the bulk gap, in contrast to the TB results of Frauenheim *et al.*[13] and Gavrilenko.[74] This means that the semiempirical TB calculations should be interpreted with some care, even if the Hamiltonian is adjusted to reproduce the correct gap.

B. Monohydride C(100)(2×1):H surface

1. Total and layer-resolved densities of states

Figure 6 shows again the local densities of states in the adsorbed H layer, in the top four C layers, and in the bulk. The striking result is that there are no states in the gap within 3 eV from the top of the valence band. Compared to the bulk, the edge of the conduction band is slightly lowered. The states below the edge of the bulk conduction band are essentially H states. Occupied hydrogen *s* states are distributed over an interval of 15 eV from the top of the valence band, with the largest DOS between 3 and 10 eV binding energy. This means that the H orbitals interact mainly with the C *p* states. The *p* DOS's of the top C layers are somewhat modified, the sharp maximum at about 5 eV binding energy results from the interaction with the H atoms. In the (*S*3) layer, the DOS is already well converged to the bulk form. Our predicted DOS for the C(100)(2×1):H surface agrees well with the TB-LDF result of Yang, Drabold, and Adams[12] (essentially no surface states within the gap), but differs from the TB result of Gavrilenko[74] predicting bonding surface states in the lower half of the gap. Our results are also similar to those obtained for the corresponding Si surface.[22]

2. Surface states

More detailed information is again contained in the calculated dispersion relations of the surface states. Figure 7 shows the surface states determined according to the criteria defined above [criterion 1 now refers to the H layer and the top C layer, criterion 2 to the H and the *S* and (*S*1) C layers]. We find that compared to the clean surface, the occupied surface states have been moved to lower energies. Due to their strong interaction with the bulk states, they tend to be more delocalized. The empty surface states have been moved upwards and shows a strong dispersion so that the surface band intersects with the bulk conduction band. Again the comparison of the surface states defined according to the two different criteria is interesting. The empty surface states are concentrated on the H layer and the top C layer, they are formed by antibonding C-H states as is also confirmed by the analysis of their charge distribution (Fig. 8). The occupied surface states correspond mainly to bonding C-H states.

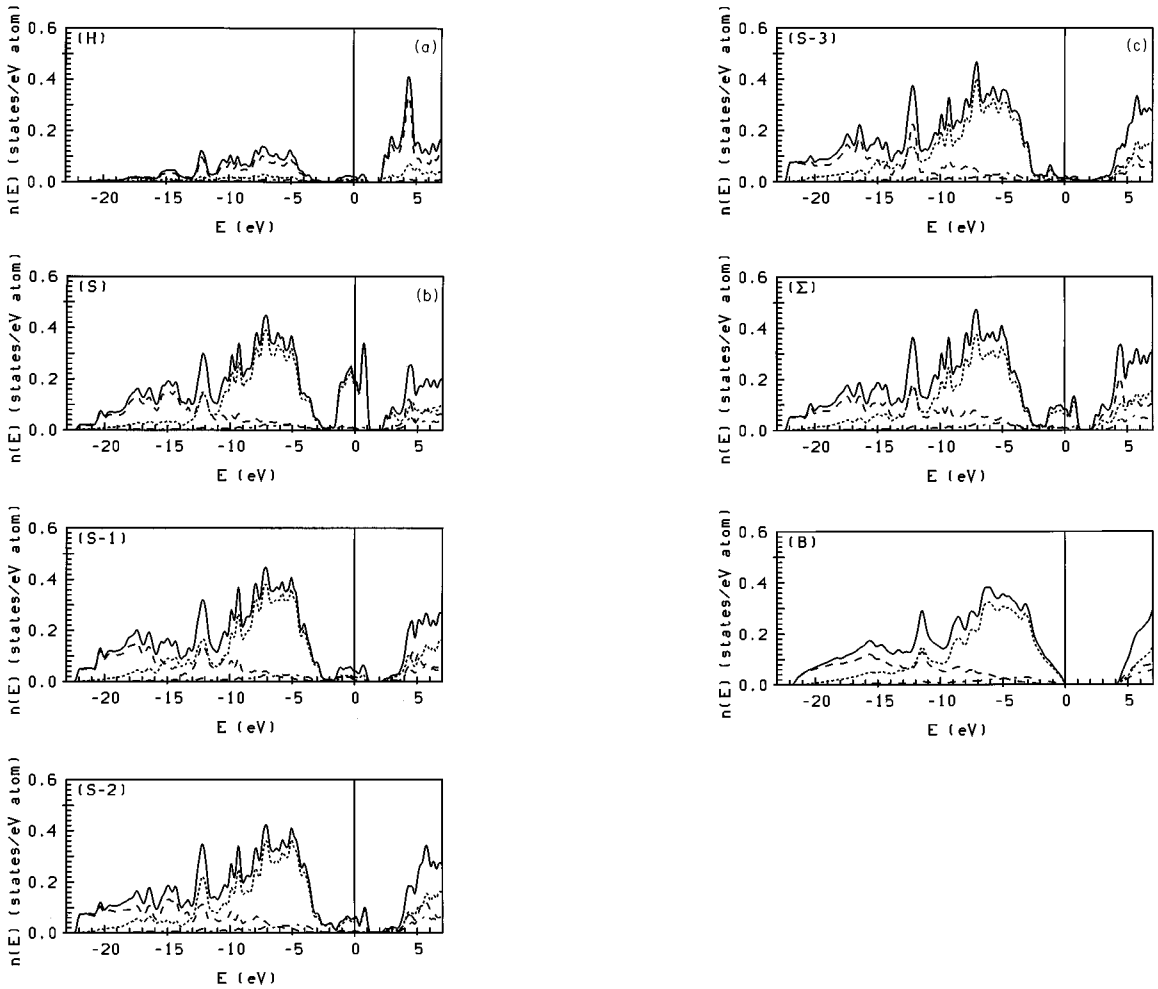

FIG. 9. Layer-resolved total and partial densities of states for the C(100)(1×1):1.5H surface. For the explanation of symbols, see Fig. 6.

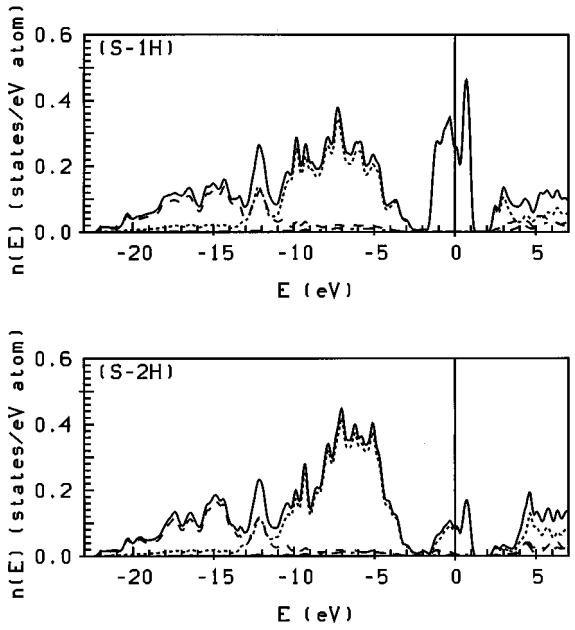

FIG. 10. Local and partial densities of states on the monohydride and dihydride C sites in the top layer of C(100)(1×1):1.5H carrying one and two H atoms, respectively. Same symbols as in Fig. 6.

A detailed analysis of the surface states shows that the hydrogenation has little effect on the states associated with σ bonds, whereas π- or $\pi^{\star}$-type surface states survive only if they fall into the bulk gap. This is demonstrated in Fig. 8. Part (a) shows the charge distribution of the strongest occupied surface state at the upper edge of the bulk band at the *S* point. The state clearly represents a C-C σ bond, weakly hybridized with the H*s* orbitals bonded to the C-C dimer. Parts (c) and (d) represent the same states as shown in Figs. 5(c) and 5(d). The eigenvalues of these states are almost unchanged; only the state shown in part (d) is somewhat more extended due to the interaction with the H *s* orbital. The lowest and most intense empty surface state [part (b)] is a $\pi^{\star}$ state, made more delocalized by interaction with the H *s* state.

For the monohydride surface, our work presents the only *ab initio* calculation of electronic surface states. We find marked differences with previous tight-binding calculations—in view of the differences that we have already discussed for the clean C(100) surface, this is not too surprising. The surface band structure calculated by Gavrilenko[74] for the monohydride surface shows an occupied and an empty surface band with weak dispersion within the bulk gap, separated by a small surface gap—this is in striking contrast to the present results and to experiment. The results of Davidson and Pickett[15] are closer to the *ab initio* predictions, but the bottom of the empty surface band at Γ almost coincides with the bottom of the bulk conduction band. This may be the conse-quence of a large C-H transfer integral leading to an overestimate of the C-H bonding-antibonding splitting.

C. Dereconstructed C(100)(1×1):1.5H surface

For the electronic properties of a C(100) surface with more than monolayer coverage of hydrogen, conflicting reports exists in the literature. Yang, Drabold, and Adams[12] report TB-LDF calculations and claim that the surface DOS of a C(100)(3×1):1.33H surface (consisting of alternating rows of H-C-C-H dimers and dihydride units) ''is essentially the same as that of the C(100)(2×1):H surface''; i.e., it shows no occupied surface states in the bulk gap. This is in contrast with the TB work of Gavrilenko[74] who find filled surface states on clean C(100)(2×1), but not on the

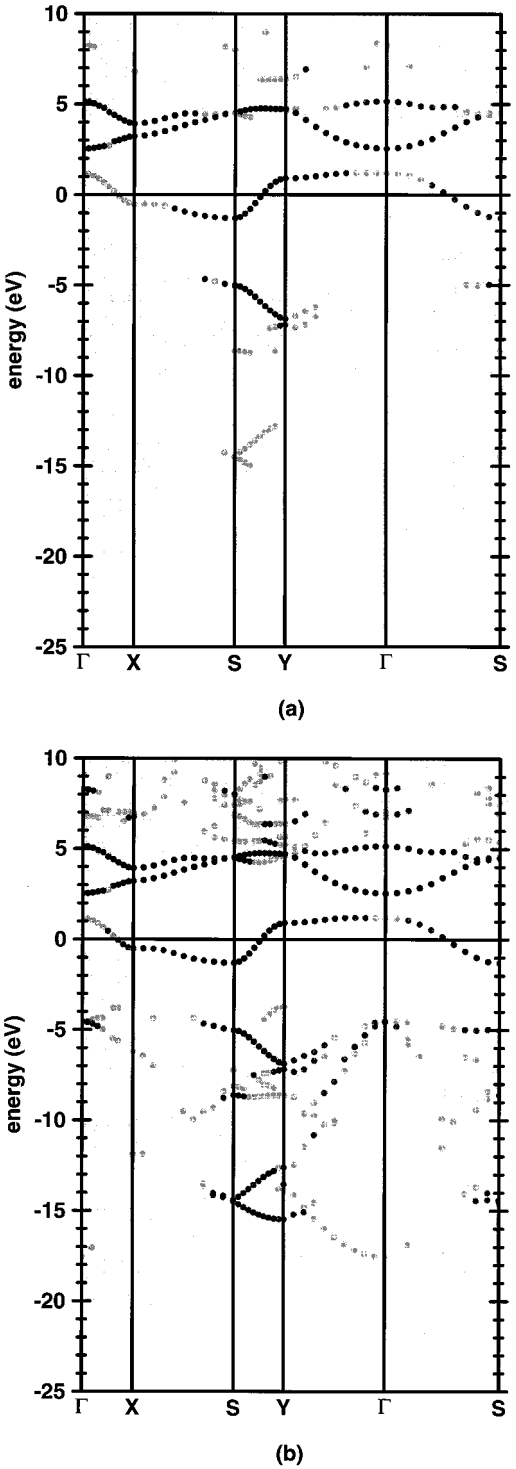

FIG. 11. Dispersion relations of electronic surface states on C(100)(1×1):1.5H, defined according to criteria (1) and (2) (a),(b). For the explanation of symbols, see Fig. 4.

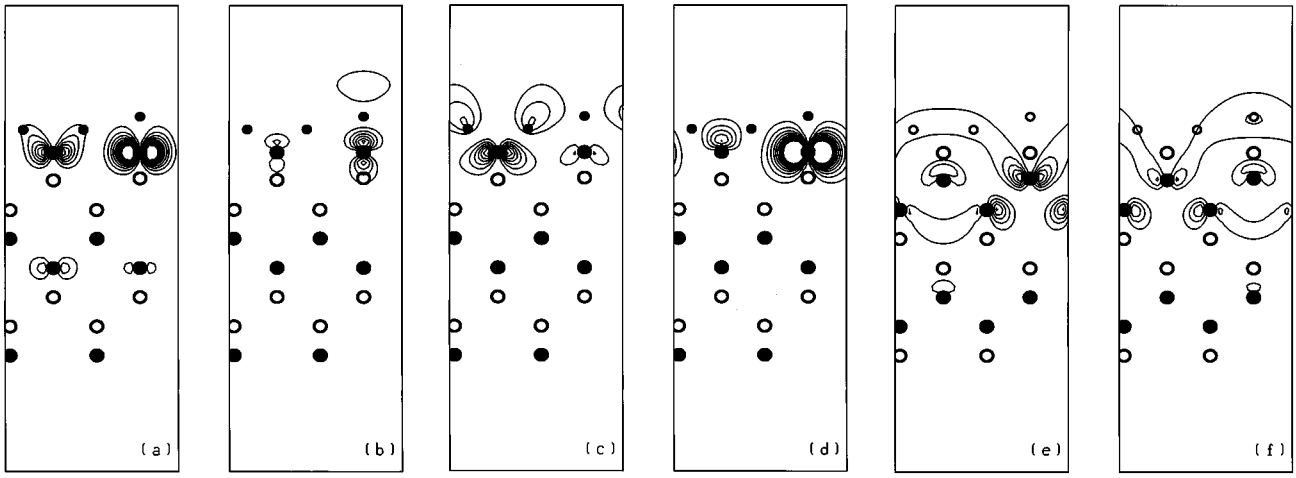

FIG. 12. Charge density distributions for electronic surface states on C(100)(1×1):1.5H. (a)–(c): Empty surface states at the Γ point and $E=1.2$ eV (a), $E=2.6$ eV (b), and $E=5.1$ eV (c). (d) Occupied state at the S point in the surface band crossing the Fermi level ($E=-1.2$ eV). (e),(f) Degenerate empty surface states at the S point and $E=4.5$ eV. Contour lines are drawn at intervals of 0.04 electrons/Å^3; cf. text.

C(100)(1×1):2H dihydride surface. Davidson and Pickett[15] report band structures for C(100):xH surfaces with varying coverages [$x=0.5$ and 1 with (2×1) periodicity and asymmetric and symmetric C dimers, respectively, and $x=1.5$ and 2 with (1×1) periodicity; cf. also Table I]. Surface states in the gap are found for $x=0.5$ and 1.5, but not for $x=1$. For $x=2$ two bands of empty surface states (consisting essentially of antibonding H states) just below the minimum of the conduction band are predicted.

1. Total and layer-resolved densities of states

Figure 9 shows the total and layer-resolved DOS for the surface with 1.5 ML coverage, arranged in the usual way. Figure 10 shows the local DOS on the monohydride and dihydride C sites in the top layer. We find a relatively large intensity in the gap, arising mainly from unsaturated dangling bond C p states on the monohydride positions, interacting with H states.

2. Surface states

Figure 11 shows the dispersion relations of electronic surface states on C(100)(1×1), classified according the criteria defined above. Within the bulk gap we find a half-occupied surface band located mainly on the top C layer and two empty surface bands consisting of C-H antibonding states. A detailed analysis shows that all states within the gap are associated with the C p orbitals on the monohydride units. The three surface states at the Γ point are located above the Fermi level [see Figs. 12(a)–12(c)]. In the sequence of increasing energies they correspond to (a) C p orbitals parallel to the surface, weakly hybridzed with H s orbitals on the dihydride, but not on the monohydride sites; (b) antibonding states formed by H s and C p_x orbitals in the monohydride units; (c) antibonding states formed by C orbitals parallel to the surface and H s orbitals on the dihydride units. The most localized occupied surface state at the S point is essentially an unsatisfied p orbital on the monohydride C site. The empty surface states at the S point [Figs. 12(e) and 12(f)] are already quite extended; they correspond mainly to antibonding linear combinations of p orbitals on the ($S1$) and ($S2$) C atoms, hybridized with Hs states of the dihydride units.

The combined evidence from our *ab initio* calculations and from the tight-binding work of Yang, Drabold, and Adams,[12] Davidson and Pickett,[15] and Gavrilenko[74] suggests that for the polyhydride surfaces states in the bulk gap appear when the existence of monohydride units is assumed, but disappear when the monohydride units are combined in H-C-C-H dimers.

D. Comparison with photoelectron spectra

We now turn to the comparison of our surface band structure with the available photoemission work. The most detailed information is given in the work of Oelhafen and Francz.[32] The (100) surfaces of natural semiconducting type-IIb diamond were investigated via ultraviolet photoelectron spectroscopy. The as-received surfaces were probably hydrogen saturated and showed no prominent surface features in the bulk gap or close to the valence-band maximum. Upon annealing at temperatures between 750 and 1250 K, a strong surface peak developed at 1.5 eV below the Fermi energy (0.5 eV below the valence-band maximum). The intensity of the surface peak was strongly reduced by reloading the surface with deuterium, but it did not completely disappear. Probably the deuterium partial pressure used in the rehydrogenation experiment [up to 21 000 L (1 L$=10^{-6}$ Torr s)] was not sufficiently high to induce a complete monolayer coverage.

Comparison of the calculated electronic density of states with experiment requires some assumptions on the escape depth of the photoelectrons and on the partial photoionization cross sections. Here we simply compare the layer-resolved DOS, integrated over the four top C layers [S to ($S3$)], plus eventually the adsorbed H layer, with the measured normal-emission photoelectron intensity. No broadening to account for the limited experimental resolution has been applied. Figure 13 shows the DOS calculated for the

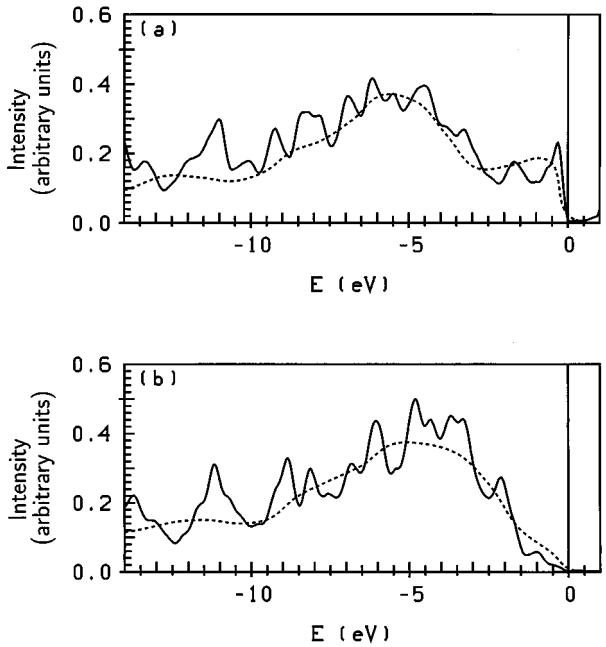

FIG. 13. (a) Photoemission intensity measured for the as-received (probably monohydrogenated) C(100) surface, compared with the local DOS integrated over the top four C layers and the H-layer of a C(100)(2×1):H surface. (b) Photoemission intensity measured for a C(100) surface annealed at 1250 K, compared with the local DOS integrated over the top four C layers of a clean C(100)(2×1) surface; cf. text.

monohydride surface compares well with the photoelectron spectrum of the as-received sample, whereas the DOS calculated for the clean surface gives a good account of the spectrum measured on the annealed sample. This confirms the interpretation of Oelhafen and Francz that high-temperature annealing leads to the formation of a hydrogen-free surface. The difference curves (Fig. 14) demonstrate that theory and experiment agree in showing that H desorption results in the appearance of surface states within an interval of 2 eV below the valence-band maximum, and a decreased DOS in the range between 2 and 5 eV binding energy. The desorption has no appreciable effect on the states at higher binding energy.

The results of Oelhafen and Francz[32] are in contrast to the photoemission experiments performed by Hamza, Kubiak, and Stulen[6] at very low photon energies ($h\nu = 6.45$ eV). Hamza, Kubiak, and Stulen found no surface states in the bulk gap for a C(100)(1×1) surface (probably a polyhydride surface), but a strong surface-state intensity over a 1.5 eV energy range *above* the valence-band maximum for a C(100)(2×1) surface. This is at variance with both theory and the experiment of Oelhafen and Francz, placing the surface states below the valence-band maximum. However, Hamza, Kubiak, and Stulen determine the position of the valence-band maximum relative to the polyhydride C(100)(1×1) surface and not relative to the monohydride C(100)(2×1) surface. As the rest of the valence band is not probed in the experiment of Hamza, Kubiak, and Stulen, it is difficult at the moment to correctly relate the energy scales of the two experiments.

Another important result is that in a two-photon photoemission experiment Hamza, Kubiak, and Stulen found no empty surface states in the bulk gap for either the (1×1) or the (2×1) surfaces. Even if we assume that the (2×1) surface had a monolayer coverage of hydrogen, this result is in contrast to all existing calculations on clean or monohydride surfaces. The source of the discrepancy could again be in the correct location of the valence-band maximum. For the (1×1) surface the reported absence of surface states in the gap would mean that we have to explore other surface structures allowing for a better saturation of dangling-bond states than our present model.

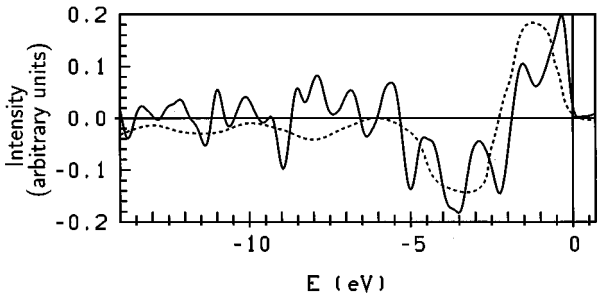

FIG. 14. Differences in the photoelectron intensities measured for the clean and hydrogen-covered C(100) surfaces (dashed line), compared with the difference in the DOS calculated for the clean and H-passivated surfaces; cf. Fig. 13 and text.

Oelhafen and Francz were also able to derive at least some information on the dispersion of the surface states by recording ultraviolet photoemission spectroscopy (He II) spectra of the annealed (clean) surface as a function of the polar angle. Variation of the angle affects mainly the states with binding energies up to 4 eV. At polar angles greater than 5°, the surface peak begins to split into two features, one is almost independent of the angle, whereas the second shifts by about 1 eV to greater binding energy. This corresponds rather well to the weak dispersion predicted for $\overline{\Gamma X}$ and the strong dispersion along the $\overline{\Gamma S}$ and $\overline{\Gamma Y}$ directions.

Angular-resolved spectra for C(100) have also been reported by Wu *et al.*[68]

E. Negative electron affinity effects

A semiconductor surface has a NEA if the vacuum level lies below the conduction-band minimum. Therefore electrons of low kinetic energy can escape from the surface and are observed in a photoemission experiment.[69,32] NEA effects may be explored in *ab initio* calculations. The vacuum level is determined from the self-consistent, plane-averaged potential in the vacuum region between the slabs. The position of the conduction-band minimum is obtained by adding to the plane-averaged self-consistent potential in the slab the difference between the average self-consistent potential and the highest occupied energy level in the bulk and the width of the bulk gap. However, at this stage we have to consider that the local-density approximation systematically underestimates the width of the gap. Therefore it is more appropriate to use the experimental value for the gap, $E_g = 5.47$ eV. This construction is shown in Fig. 15 for a slab consisting of eight C layers and eight equally wide vacuum layers (similar results are obtained for a 16+16 layer slab). One side of the slab is fixed in the bulk geometry and one side relaxed

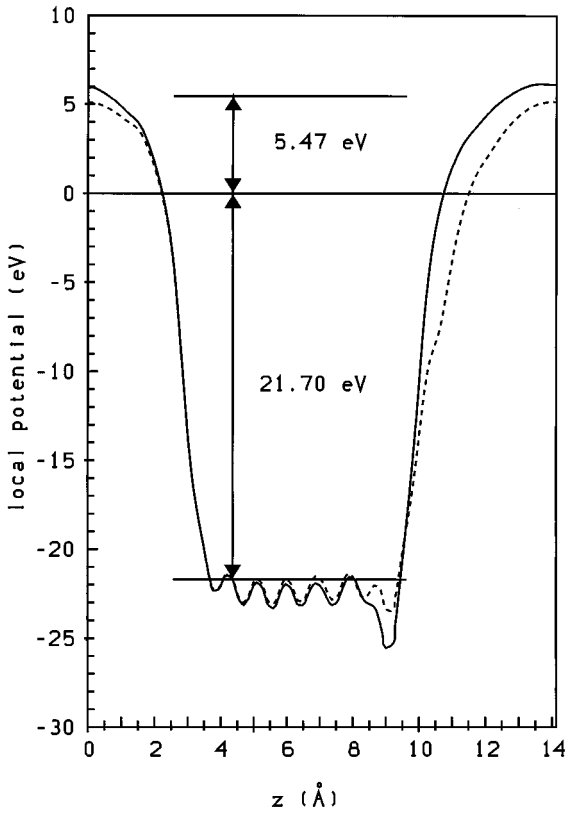

FIG. 15. Calculated plane-averaged selfconsistent potentials for clean (full lines) and monohydrogenated (dashed line) C(100)(2×1) surfaces. The positions of the valence-band maximum and the conduction-band minimum in the bulk are indicated; cf. text.

with or without a covering H layer. We find, in agreement with van der Weide *et al.*[69] that a NEA is found for the C(100)(2×1):H surface, but not for the clean surface. The difference has to be attributed to the existence of a much stronger dipole layer on the clean surface arising from the charge distribution of the dangling-bond orbitals in the surface states.

VI. DISCUSSION AND CONCLUSIONS

Using the *ab initio* molecular-dynamics package VAMP we have been able to perform a thorough study of the structural and electronic properties of clean and hydrogenated diamond (100) surfaces. We find that the clean surface reconstructs in a (2×1) cell via the formation of rows of symmetric dimers. The C-C bond length in the dimers is $d_{C-C}=1.37$ Å, almost exactly equal to the length of a C=C double bond in hydrocarbon molecules. The symmetric dimer reconstruction contrasts the formation of asymmetric surface dimers on Si(100) and Ge(100) surfaces. The origin of this difference is in the different character of the electronic surface states. On Si(100) with symmetric dimers the occupied and empty surface bands are formed mostly by dangling-bond orbitals with only a weak π interaction to form the bonding π and antibonding $\pi^\star$ bands and no surface band gap at the Fermi level. This favors a Jahn-Teller-like distortion leading to asymmetric dimers and the formation of a surface band gap. On C(100) the occupied and empty surface bands are formed by bonding π and antibonding $\pi^\star$ linear combinations of the dangling-bond orbitals, rehybridized to some degree with σ orbitals (see Fig. 5). There is no overlap between the states localized at neighboring dimers. The much stronger π interaction leads to the formation of a surface band gap already for symmetric dimers and prevents a Jahn-Teller distortion. Further surface bands are associated with the σ bonds in the dimers. Due to the very strong σ interaction the bonding σ surface band occurs within the projected bulk band structure.

A monolayer coverage of hydrogen transforms the double bond in the dimer into a single bond (as reflected by the increase in the dimer bond length to $d_{C-C}=1.61$ Å), but preserves the (2×1) periodicity of the surface. The hydrogen passivation of the dangling-bond orbitals eliminates the π-bonded surface states from the gap and shifts the $\pi^\star$ states to higher energies. The σ-bonded states are almost unaffected.

Very recent photoemission experiments[32] confirm the existence of an occupied surface band with a maximum coinciding with the maximum of the bulk valence band and a dispersion of about 1.7 eV. The calculation predicts that passivation with a monolayer of H eliminates the surface-related intensity in the interval between the Fermi level and 2-eV binding energy and increases the density of states in the interval between 2- and 5-eV binding energy. Again this is in full agreement with the measured photoelectron spectra. The presently available experimental information does not allow a critical assessment of the theoretical prediction relating to empty surface states. Investigations by inverse photoemission spectroscopy seem to be highly desirable.

If corrected for the local-density error in the prediction of the bulk gap, the theory correctly predicts a negative electron affinity for the hydrogenated but not for the clean C(100) surface, in agreement with experiment.[69] The difference has to be attributed to the strong dipole potential that exists on the clean, but not on the hydrogenated surface.

Whereas the theory gives a consistent and satisfactory picture of the properties of the clean and monohydrogenated surfaces, some questions concerning the nature of the unreconstructed polyhydride C(100)(1×1):*x*H surface remain. In our work we have studied a model with a 1.5 ML coverage consisting of alternating rows of monohydride and dihydride units. We have found that this structure is at least metastable in a relaxed configuration with a (1×1) periodicity in the C surface layer. The desorption energy from the C(100)(1×1):1.5H to the reconstructed C(100)(2×1):H surface is predicted as $\Delta E_H = 1.02$ eV/H atom, i.e., much lower than the desorption energy from the monohydrogenated C(100)(2×1):H to the clean C(100)(2×1) surface of $\Delta E_H = 4.54$ eV/H atom. This corresponds rather well to the two-stage desorption process observed by Hamza, Kubiak, and Stulen[6] by electron-stimulated thermal desorption experiments. However, this structure leads to the formation of a partially occupied surface band at the Fermi level. The prediction of a metallic surface state does not agree with the photoelectron spectroscopy of Hamza, Kubiak, and Stulen[6] for C(100)(1×1):*x*H surfaces. The possibility that other surface structures are energetically more favorable cannot be excluded at present. A definite answer to that question seems to require a dynamical simulation of the strongly hydrogenated surface in which the hydrogen atoms are allowed to move freely and to adopt the energetically most favorable

positions with a few symmetry constraints as possible. This, however, must be left to future work.

ACKNOWLEDGMENTS

This work has been supported by the Austrian Science Foundation (Fonds zur Förderung der wissenschaftlichen Forschung in Österreich) within the framework of the trinational German-Austrian-Swiss Research Cooperation on Superhard Materials (D-A-CH), project No. SJ908. Stimulating discussions with Professor P. Oelhafen (Basel) and Professor L. Ley (Erlangen) within the D-A-CH workshops are gratefully acknowledged.

[1] Ch. Wild, N. Herres, and P. Koidl, J. Appl. Phys. **68**, 973 (1990).
[2] See, e.g., the articles in *SiC, Natural and Synthetic Diamond and Related Materials*, edited by A.A. Gippius, R. Hellbrig, and J.P.F. Sellschop (North-Holland, Amsterdam, 1992).
[3] K.E. Spear and M. Frenklach, Pure Appl. Chem. **66**, 1773 (1994).
[4] C.J. Chu, M.P. d'Evelyn, R.H. Hauge, and J.L. Margrave, J. Appl. Phys. **70**, 1695 (1991).
[5] B.B. Pate, Surf. Sci. **165**, 83 (1986).
[6] A.V. Hamza, G.D. Kubiak, and R.H. Stulen, Surf. Sci. **237**, 35 (1990).
[7] D. Reichardt and F. Bechstedt, Surf. Sci. **202**, 83 (1988).
[8] D.W. Brenner, Phys. Rev. B **42**, 9458 (1992).
[9] X.M. Zheng and P.V. Smith, Surf. Sci. **250**, 369 (1991).
[10] S.P. Mehandru and A.B. Anderson, Surf. Sci. **248**, 369 (1991).
[11] Y.L. Yang and M.P. d'Evelyn, J. Vac. Sci. Technol. A **10**, 978 (1992).
[12] S.H. Yang, D.A. Drabold, and J.B. Adams, Phys. Rev. B **48**, 5261 (1993).
[13] T. Frauenheim, U. Stephan, P. Blaudeck, D. Porezag, H.G. Bussmann, W. Zimmermann-Edling, and S. Lauer, Phys. Rev. B **48**, 18 189 (1993).
[14] S. Skokov, C.S. Carmer, B. Weiner, and M. Frenklach, Phys. Rev. B **49**, 5662 (1994).
[15] B.N. Davidson and W.E. Pickett, Phys. Rev. B **49**, 11 253 (1994).
[16] D. Haneman, Rep. Prog. Phys. **50**, 1045 (1987).
[17] J.E. Northrup, Phys. Rev. B **44**, 1419 (1991).
[18] K. Kobayashi, Y. Morikawa, K. Terakura, and S. Blügel, Phys. Rev. B **45**, 3469 (1992).
[19] J.E. Northrup, Phys. Rev. B **47**, 10 032 (1993).
[20] J. Dabrowski and M. Scheffler, Appl. Surf. Sci. **56**, 15 (1992).
[21] Z. Jing and J. L. Whitten, Phys. Rev. B **46**, 9544 (1992).
[22] A. Vittadini, A. Selloni, R. Car, and M. Casarin, Phys. Rev. B **46**, 4328 (1992).
[23] A. Vittadini, A. Selloni, and M. Casarin, Phys. Rev. B **49**, 11 191 (1994).
[24] M. Needles, M.C. Payne, and J.D. Joannopoulos, Phys. Rev. Lett. **58**, 1765 (1987).
[25] L. Spiess, A.J. Freeman, and P. Soukiassian, Phys. Rev. B **50**, 2249 (1994).
[26] J. Furthmüller, J. Hafner, and G. Kresse, Europhys. Lett. **28**, 659 (1994).
[27] C. Kress, M. Fiedler, W.G. Schmidt, and F. Bechstedt, Phys. Rev. B **50**, 17 697 (1994).
[28] P. Krüger and J. Pollmann, Phys. Rev. Lett. **74**, 1155 (1995).
[29] Z. Jing and J.L. Whitten, Phys. Rev. B **50**, 2598 (1994).
[30] P.G. Lurie and J.M. Wilson, Surf. Sci. **65**, 453 (1977).
[31] R. Graupner, J. Ristein, and L. Ley, Surf. Sci. **320**, 201 (1994).
[32] P. Oelhafen and G. Francz (private communication); G. Francz and P. Oelhafen, Surf. Sci. **329**, 193 (1995).
[33] G. Kresse and J. Hafner, Phys. Rev. B **47**, 558 (1993); **48**, 13 115 (1993).
[34] G. Kresse and J. Hafner, Phys. Rev. B **49**, 14 251 (1994).
[35] G. Kresse and J. Furthmüller (unpublished).
[36] D. Vanderbilt, Phys. Rev. B **41**, 7892 (1990).
[37] G. Kresse and J. Hafner, J. Phys. Condens. Matter **6**, 8245 (1994).
[38] For a recent discussion of convergence problems in pseudopotential calculations of diamond surfaces, see W.G. Schmidt, A. Scholze, and F. Bechstedt, Surf. Sci. (to be published).
[39] N.D. Mermin, Phys. Rev. **137**, A1441 (1965).
[40] J.P. Perdew and A. Zunger, Phys. Rev. B **23**, 5048 (1981).
[41] M.P. Teter, M.C. Payne, and D.C. Allan, Phys. Rev. B **40**, 12 255 (1989).
[42] R.D. King-Smith, M.C. Payne, and J.S. Lin, Phys. Rev. B **44**, 13 063 (1991).
[43] T.A. Arias, M.C. Payne, and J.D. Joannopoulos, Phys. Rev. B **45**, 1538 (1992).
[44] M.C. Payne, M.P. Teter, D.C. Allan, T. A. Arias, and J.D. Joannopoulos, Rev. Mod. Phys. **64**, 1045 (1992).
[45] D.M. Bylander, L. Kleinman, and S. Lee, Phys. Rev. B **42**, 1394 (1990).
[46] C.G. Broyden, Math. Comput. **19**, 577 (1965).
[47] G. Kresse, thesis, Technische Universität, Wien, 1993.
[48] D.D. Johnson, Phys. Rev. B **38**, 12 087 (1988).
[49] S. Blügel, thesis, Technische Hochschule, Aachen, 1989.
[50] G. Kresse, in Proceedings of the 6th International Conference on the Structure of Non-Crystalline Materials, Prague, 1994, edited by L. Cervinka and A.C. Wright [J. Non-Cryst. Solids **192 & 193**, 222 (1995)].
[51] J. Furthmüller, J. Hafner, and G. Kresse, Phys. Rev. B **50**, 15 606 (1994).
[52] G.B. Bachelet, D.R. Hamann, and M. Schlüter, Phys. Rev. B **26**, 4199 (1982).
[53] A.M. Rappe, K.M. Rabe, E. Kaxiras, and J.D. Joannopoulos, Phys. Rev. B **41**, 1227 (1990).
[54] J.L. Lin, A. Qteish, M.C. Payne, and V. Heine, Phys. Rev. B **47**, 4174 (1993).
[55] G. Kresse, J. Hafner, and R.J. Needs, J. Phys. Condens. Matter **4**, 7451 (1992).
[56] H.J. Monkhorst and J.D. Pack, Phys. Rev. B **13**, 5188 (1976); D.J. Chadi and M.L. Cohen, *ibid.* **8**, 5747 (1973).
[57] A. de Vita and M.J. Gillan, J. Phys. Condens. Matter **3**, 6225 (1991).
[58] M. Methfessel and A. Paxton, Phys. Rev. B **40**, 3616 (1989).
[59] A. Eichler, J. Hafner, G. Kresse, and J. Furthmüller, Surf. Sci. **346**, 300 (1996).
[60] A. Vittadini, A. Selloni, and M. Casarin, Surf. Sci. Lett. **289**, L625 (1993).
[61] J.J. Boland, Surf. Sci. **261**, 17 (1992).
[62] M. Winn and M. Rassinger, Europhys. Lett. **32**, 55 (1995).
[63] F. J. Himpsel, D. E. Eastman, P. Heimann, and J. F. van der Veen, Phys. Rev. B **24**, 7270 (1981).

[64] S. Iarlori, G. Galli, F. Gygi, M. Parrinello, and E. Tosatti, Phys. Rev. Lett. **69**, 2947 (1992).
[65] C. Kress, M. Fiedler, and F. Bechstedt, Europhys. Lett. **28**, 433 (1994).
[66] F. Ancilotto, W. Andreoni, A. Selloni, R. Car, and M. Parrinello, Phys. Rev. Lett. **65**, 3148 (1990).
[67] F. Ancilotto and A. Selloni, Phys. Rev. Lett. **68**, 2640 (1992).
[68] J. Wu, R. Cao, X. Yang, P. Pianetta, and D. Lindau, J. Vac. Sci. Technol. A **11**, 1048 (1993).
[69] J. van der Weide, Z. Zhang, P.K. Baumann, M.G. Wensell, J. Bernholc, and R.J. Nemanich, Phys. Rev. B **50**, 5083 (1994).
[70] F.J. Himpsel, J.A. Knapp, J.A, van Vechten, and D.E. Eastman, Phys. Rev. B **20**, 624 (1979).
[71] J. van der Weide and R.J. Nemanich, J. Vac. Sci. Technol. B **10**, 1940 (1992).
[72] B.B. Pate, M.H. Hecht, C. Binns, I. Lindau, and W.E. Spicer, J. Vac. Sci. Technol. **21**, 364 (1982).
[73] D. Krüger and J. Pollmann, Phys. Rev. B **47**, 1898 (1993).
[74] V.I. Gavrilenko, Phys. Rev. B **47**, 9556 (1993).
[75] C.D. Clark, P.J. Dean, and P.V. Harris, Proc. R. Soc. London Ser. A **227**, 312 (1964).
[76] L. Hedin and S. Lundqvist, Solid State Phys. **23**, 1 (1969).
[77] M.S. Hybertsen and S.G. Louie, Phys. Rev. B **34**, 5390 (1986).